ACS OMEGA

Open Access

http://pubs.acs.org/journal/acsodf

Article

Evaluation of the Combinatory Anticancer Effect of Chemotherapeutic Compounds and Prodigiosin against HCT-116, LoVo, and A549 Cell lines

Fares Elghali, Dhouha Msalbi, Fakher Frikha, Mona Alonazi, Emna Sahli, Bochra Hakim, Sami Mnif, Abir Ben Bacha,* and Sami Aifa

Cite This: *ACS Omega* 2024, 9, 48112−48124

Read Online

ACCESS | Metrics & More | Article Recommendations

ABSTRACT: Despite their wide usage in reducing tumors and improving patients' survival, chemotherapeutic drugs or natural compounds are facing the development of cancer resistance. Many experimental data and clinical trials have shown that combinatorial treatment could be an efficient solution for some resistance problems. In this study, we aimed to evaluate the synergistic effects of combining prodigiosin (PG), a natural compound with known anticancer properties, with the commonly used chemotherapy drugs 5-fluorouracil (5-FU), oxaliplatin, and paclitaxel. The primary objective was to identify the most potent combination that could enhance tumor cytotoxicity while minimizing drug resistance. *In vitro* experiments using three cancer cell lines (LoVo, HCT-116, and A549) were conducted to assess the impact of these combinations on the cell viability and proliferation. Recorded data demonstrated that the combination of 20 μM PG with 1/2 IC50 of 5-FU showed the most significant decrease in cell viability, with remaining viabilities of 28, 32, and 43% for LoVo, HCT-116, and A549 cells, respectively. This combination resulted in a notable increase in the proportion of cells in the G0/G1 phase and a decrease in the S phase of the cell cycle. These findings indicated that this combination effectively induced cell-cycle arrest. In contrast, other combinations such as PG with paclitaxel or oxaliplatin were less effective. Furthermore, molecular docking studies revealed that PG targets Akt1, a key protein in the PI3K/Akt survival pathway, providing a possible explanation for its proapoptotic effects. These findings suggested that the combination of PG with 5-FU enhanced tumor cell sensitivity to chemotherapy, potentially offering a more effective treatment strategy for overcoming drug resistance. In conclusion, the current study highlighted the promising potential of PG in combination with 5-FU as a therapeutic approach for colorectal and lung cancers, warranting further investigations in preclinical and clinical settings.

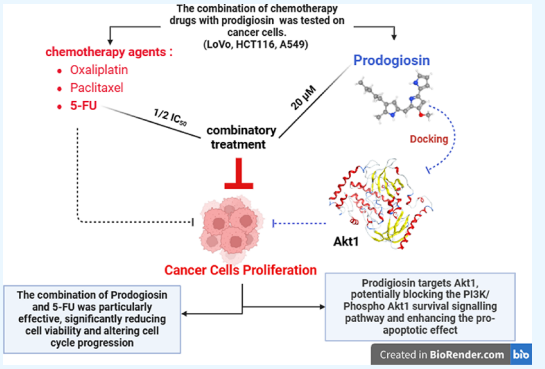

HIGHLIGHTS

1. The combination of different chemotherapeutic agents is an effective strategy for optimizing tumor cytotoxicity in cancer treatment.
2. The combinatorial treatment of 20 μM of PG + 1/2 IC50 of 5-FU showed the best significant viability decrease in cancer cells.
3. The combination of PG with 5-FU increased the percentage of cells in the G0/G1 phase and decreased the percentage of cells in the S phase.
4. The docking studies supported targeting Akt1 in cancer by prodigiosin.

INTRODUCTION

Chemotherapy remains a critical tool in treating nonsmall cell lung cancer (NSCLC) and human colon cancer (HCC).[1,2] However, ongoing research into the genetic and molecular underpinnings of drug resistance is essential for improving patient outcomes and developing more effective therapeutic strategies, such as EGFR mutations in some NSCLC patients and K-Ras mutations in HCC,[3,4] in addition to activation of alternative cancer signaling pathways. Moreover, cancer cells can increase the expression of efflux pumps, such as P-glycoprotein, which actively pump chemotherapy drugs out of the cells.[5,6] Increased expression of these pumps reduces the intracellular concentration of the drugs, limiting their effectiveness.[6−8] Also, cancer cells can activate survival pathways, such as the PI3K/

Received: May 20, 2024
Revised: November 1, 2024
Accepted: November 15, 2024
Published: November 26, 2024

https://doi.org/10.1021/acsomega.4c04760
ACS Omega 2024, 9, 48112−48124

Table 1. IC50 Determination for the PG, 5-FU, Paclitaxel, and Oxaliplatin in LoVo, HCT-116, and A549 Cells after 48h (the Results (mean ± SD) Are Representative of Three Independent Experiments)

	IC 50 (μM)			
	LoVo	HCT-116	A549	Hek293
PG	68.12 ± 0.23	62.81 ± 2.36	80.36 ± 1.78	>100
5-FU	19.99 ± 3.21	26.98 ± 1.87	37.58 ± 1.25	11.86 ± 2.23
paclitaxel	90.52 ± 0.25	73.09 ± 3.47	71.09 ± 2.14	
oxaliplatin	19.51 ± 1.02	13.48 ± 0.87	82.64 ± 1.65	

AKT/mTOR signaling,[9−11] which promotes cell survival to malignant cells, making them less susceptible to the cytotoxic effects of chemotherapy drugs.[9,12,13] The tumor microenvironment, including factors like hypoxia and interactions with stromal cells, can contribute to chemotherapy resistance in NSCLC[14,15] and human colon cancer.[5−7] In fact, hypoxic regions within tumors have been associated with resistance to certain chemotherapy drugs. These drugs often work through damaging the DNA of cancer cells, and inducing their death, however, malignant cells, can improve their DNA repair capabilities.[8,9]

Chemotherapy, often referred to as "chemo", is a type of cancer treatment that uses drugs to destroy or slow down the growth of cancer cells. It may be used alone or in combination with other treatments such as surgery, radiation therapy, or immunotherapy, depending on the type and stage of cancer. 5-Fluorouracil (5-FU), oxaliplatin, and paclitaxel chemo drugs are commonly used in the treatment of various tumors, particularly colorectal cancer. Oxaliplatin is a platinum-based chemotherapy drug that works by interfering with the DNA of cancer cells, preventing them from dividing and growing.[10,11] It is often used in combination with other chemotherapy drugs for HCC treatment. Paclitaxel belongs to a class of chemotherapy drugs known as taxanes that work by stabilizing microtubules in cells that are crucial for cell division, which prevents the growth of cancer cells. Paclitaxel is used in the treatment of various cancers, including breast, ovarian, and lung cancers. 5-FU is a type of antimetabolite that interferes with the synthesis of DNA and RNA and commonly used in the treatment of colorectal cancer and other gastrointestinal cancers.[12−14] 5-FU is incorporated into the DNA and RNA molecules, disrupting their normal function and inhibiting the division of cancer cells. By inhibiting cell growth, 5-FU helps to slow down or shrink tumors.[12]

Several new studies have shown that some secondary metabolites produced by bacteria could have antiproliferative effects on cancer cells. For instance, prodigiosin (PG), a deep red secondary metabolite with a Tripyrrole structure, was first extracted and characterized from the bacterium *Serratia marcescens*.[15] PG has been shown to exert antimicrobial, antimalarial, and immunosuppressive properties[16] and has also demonstrated antibacterial effects against both Gram-positive and Gram-negative bacteria.[17] Interestingly, PG has a promising activity against various types of cancer cells, including breast, lung, and colon.[7,17−19] Consequently, PG and its synthetic analog obatoclax have been tested in several preclinical and clinical trials alone or in combination with conventional chemotherapeutics as anticancer agents.[18,20] In that respect, different effects on both apoptosis and autophagy have been observed in various cancer models. The exact mechanism of action of PG is not fully understood, but it is believed to involve disruption of DNA and inhibition of various cellular processes.[21] However, further research is still needed to fully understand its therapeutic potential and ensure its safety for human use. The use of combinatory therapeutic approaches plays a significant role in cancer treatment, aimed at improving treatment outcomes and overcoming various challenges.[22,23]

The combinatory approaches discussed aim to target cancer cells through multiple mechanisms, enhancing treatment response, reducing the likelihood of resistance, and improving overall patient outcomes. Importantly, combining chemical therapies with natural compounds is a promising but complex strategy. Its effectiveness depends on factors, such as cancer type, stage, patient characteristics, treatment goals, and available therapies. The urgent need for innovative approaches to treat lung and colon cancers drives the search for effective combinations.[24,25] The mechanisms by which natural compounds synergize with 5-FU are diverse and may include the modulation of apoptosis pathways, inhibition of drug efflux pumps that remove drugs from cancer cells, suppression of drug-resistant proteins, and alteration of cellular signaling pathways. Additionally, these natural compounds can help in alleviating the side effects of chemotherapy, as some possess protective effects on normal cells, thereby reducing treatment-related toxicity. However, it is important to note that research on combining PG with chemotherapy is still in its early stages, and clinical applications remain poorly established.[26−28] This study aimed to (i) assess the synergistic effects of combining chemotherapy drugs (oxaliplatin, paclitaxel, and 5-FU) with PG on NSCLC and HCC cell lines, (ii) evaluate the impact of this combination on reducing chemotherapy drug dosage while maintaining efficacy, and (iii) investigate the interaction between PG and Akt1 using *in silico* methods to validate its potential as a therapeutic target.

MATERIALS AND METHODS

Reagents. The PG was produced and purified from *Serratia sp*. C6LB strain as previously described[17]; oxaliplatin, paclitaxel, and 5-FU were obtained from Cytopharma—pharmaceutical company (Z.I Hammam Zriba—1152 Zaghouan—Tunisia). The compounds were solubilized in DMSO as stock solutions (100 mM), and serial dilutions were prepared with cell culture media prior to use.

Cell Culture. Two colon cancer cell lines (LoVo [RRID: CVCL_0399] and HCT-116 [RRID: CVCL_0291]) and one lung cancer cell line (A549 [RRID: CVCL_0023]) were used in this study.

Cells were cultured in RPMI-1640 and DMEM media supplemented with 10% FBS, and penicillin−streptomycin were purchased from PAN BIOTECH (Germany). They were grown in a humidified incubator by ESCO with 5% of CO_2 at 37 °C. A human embryonic kidney 293 (Hek293) cell was used as a control to verify the toxicities of the PG and 5-FU. All cells are obtained from the Center of Biotechnology of Sfax-Tunisia.

Cytotoxic Activity. A 96-well plate was seeded with 5000 cells/well and incubated overnight in an incubator at 37 °C with 5% of CO_2. Next, the treatments were performed in triplicates

https://doi.org/10.1021/acsomega.4c04760
ACS Omega 2024, 9, 48112−48124

and the plate was placed back in the incubator. After 48 h, the medium was removed and 100 μL of MTT (3-(4,5-dimethylthiazol-2-yl)-2,5-diphenyltetrazolium bromide) was added into each well and incubated for 24 h. Subsequently, the MTT-containing medium was removed from the wells. A total of 100 μL of SDS 10% was added into each well to dissolve the formazan crystals from the cells. Next, the plate was analyzed on a microplate reader (Varioskan Thermo Fisher) after 4 h. The absorbance was measured for each well with a wavelength of 570 nm. The cell viability percentage of the treated cells was calculated relatively to the cell viability of the control untreated cells:

$$\textbf{cell viability ratio}\ (\%) = (\textbf{OD treated}/\textbf{OD control}) \times \textbf{100}\%$$

where OD treated is the optical density of the treated cells and OD control is the optical density of the control (untreated cell).

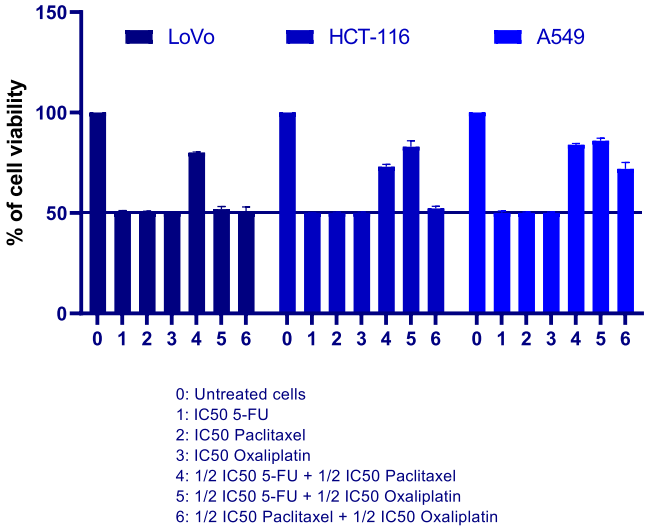

Figure 1. Chemotherapy drug combination sensitizes in LoVo, HCT-116, and A549 cells. The cells were treated with 5-FU, paclitaxel, and oxaliplatin for 48 h, and MTT assays were performed to assess cell viability. Results were presented as mean ± SD from three independent experiments.

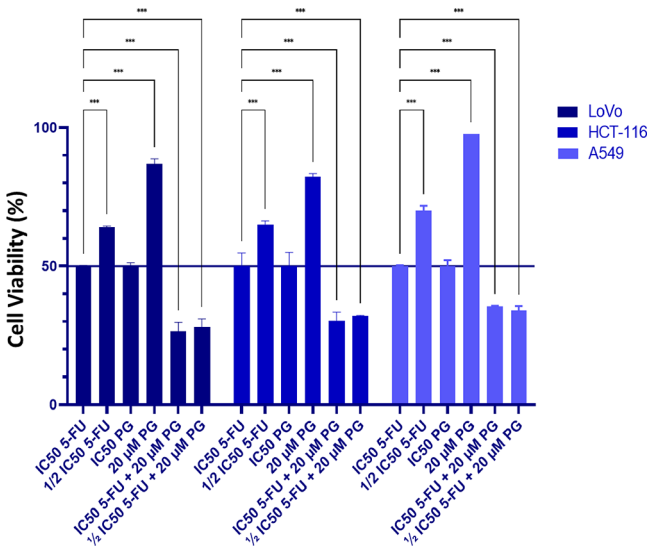

Figure 3. Effect of PG (20 μM), 5-FU, and Mix (20 μM PG + 1/2 IC50 5-FU) on human cancer cell proliferation. Cells were exposed for 48h. Results were presented as mean ± SD from three independent experiments (*p < 0.05; **p < 0.01; ***p < 0,001).

This calculation gave the percentage of viable cells after treatment compared with the control. To prepare a dose–response curve, the logarithm (usually base 10) of the treatment concentration is generally considered. The concentration values were computed according to their logarithms: Log_{10} (concentration) providing the log-transformed values for the x-axis of the survival curve. The resulting plot shows how cell viability changes with different concentrations of the treatment. The curve can help determine the concentration at which the treatment becomes effective (e.g., IC50 value).[29]

Cellular Proliferation Assay. The 5-bromo-2′-deoxyuridine (BrdU) labeling and detection kit III (Roche, catalog number: 11 444 611 001) were used for the determination of cellular proliferation. BrdU is usually incorporated into freshly synthesized DNA instead of thymidine.[30] Cancer cell lines were cultured in a 96 microtiter well plate with a final volume of 100 μL of culture medium and treated with 20 μM PG, 1/2 IC50 and IC50 of 5-FU, and Mix (20 μM PG + 1/2 IC50 5-FU). After incubation, the BrdU labeling and detection were conducted

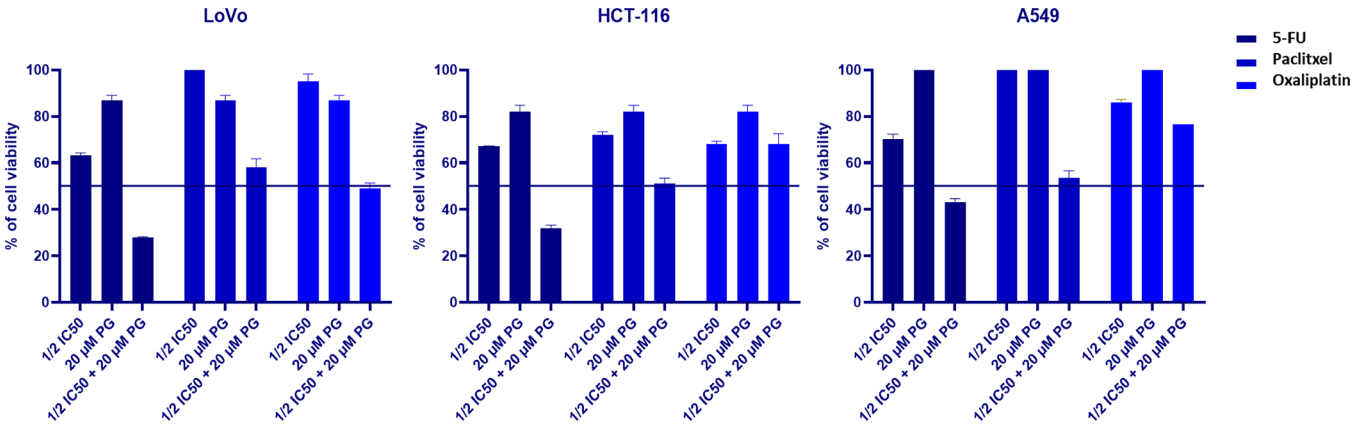

Figure 2. Prodigiosin sensitizes LoVo, HCT-116, and A549 cells to 5-FU, paclitaxel, and oxaliplatin induced cell death. The cells were treated with 1/2 IC50 of 5-FU, paclitaxel, and oxaliplatin in the presence or absence of 20 μM of PG for 48 h, and MTT assays were performed to assess cell viability. Results were presented as mean ± SD from three independent experiments.

https://doi.org/10.1021/acsomega.4c04760
ACS Omega 2024, 9, 48112−48124

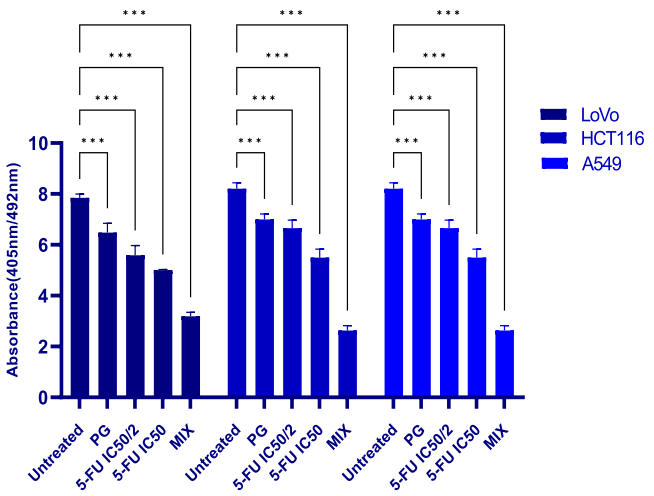

Figure 4. Effect of PG (20 μM), 5-FU, and Mix (20 μM PG + IC50/2 5-FU) on human cancer cell proliferation was evaluated using a BrdU incorporation assay. Cells were exposed for 48h. Results were presented as mean ± SD from three independent experiments (*p < 0.05; **p < 0.01; ***p < 0,001).

according to the manufacturer's instructions. BrdU labeling solution was added to the culture medium, and then cells were fixed, and DNA was partially digested by nucleases. The anti-BrdU-POD was used to detect BrdU incorporation through the colored reaction product in the presence of the peroxidase substrate ABTS. The BrdU incorporation can be quantified by normalizing the OD at 405 nm to the OD at 490 nm.

$$\textbf{BrdU incorporation} = \mathbf{OD_{405}/OD_{490}}$$

The resulting value provides an indication of the relative amount of BrdU incorporated into the DNA of the treated cells compared with the control. Higher values suggest greater cell proliferation activity as more BrdU is incorporated during DNA synthesis.

Cell Cycle. Cells were seeded in 60 mm plates at 3 × 10^5 cells/well. After 24 h of adhesion, cells were treated with 20 μM of PG and the half of the IC50 concentration (1/2 IC50) of 5-FU, and with the combination of 20 μM PG and 1/2 IC50 of 5-FU, cells were subjected to a series of preparatory steps for flow cytometry analysis.

Initially, cells were detached by trypsinization in the culture plate and rinsed with phosphate-buffered saline (PBS) to remove the residual media. Cells were then fixed in 70% cold ethanol overnight at −20 °C to preserve the cellular morphology and DNA integrity. After fixation, cells were washed twice with cold PBS to eliminate excess ethanol and resuspended in a staining solution consisting of 500 μL of PBS, 12 μL of propidium iodide (PI) at a concentration of 20 mg/mL, and 2.5 μL of RNase A (20 mg/mL). The mixture was incubated for 60 min at 37 °C in the dark to allow DNA adequate staining.

Subsequently, the samples were stored at 4 °C until analysis. Flow cytometry was performed using the Attune Nxt flow acoustic focusing cytometer (Thermo Fisher) equipped with a 488 nm argon laser. Data acquisition was set to collect 10,000 events per sample at a flow rate of 100 μL/min, utilizing linear amplification. The red fluorescence corresponding to the PI signal was detected at a wavelength of 695 ± 40 nm (channel BL3). Unstained and untreated cells served as negative and positive controls, respectively. Cell-cycle distribution was assessed by analyzing the BL3-A peak versus counts, and each assay was conducted in triplicate to ensure statistical reliability.[31]

***In Silico* Study.** *Homology Modeling and Evaluation of the Model.* The 3D structure of the Akt1 protein was built using the structure-modeling program MOE 2019 due to the incomplete detailed structural information available for the crystallized structure in the Protein Data Bank (PDB). The protein structure was used from the PDB (ID: 6S9W). The model was then subjected to molecular mechanics optimization using the CHARMM27 force field until the gradient reached 0.01 kcal/(Å.mol). The 3D target protein structure was validated using PROCHECK[32] and ERRAT[33] on SAVESv6.0 web server. PROCHECK was employed to ensure that the protein structure met established geometric standards, identifying potential distortions. ERRAT scores helped in refining the structure and provided insights into their reliability.

Molecular Docking. Protein−ligand docking was performed using the Molecular Operating Environment (MOE). Preparation of the 3D Structure of Ligands and Protein Targets: The 3D structures were built of Akt1. The three-dimensional (3D) structure of ligands such as PG (CID 135455579), ATP (CID 5957), IQO (CID 10196499), and Akt1 inhibitor VII (PubChem ID: 10196499), as well as the inhibitor evaluated, were retrieved from the PubChem compound database. The

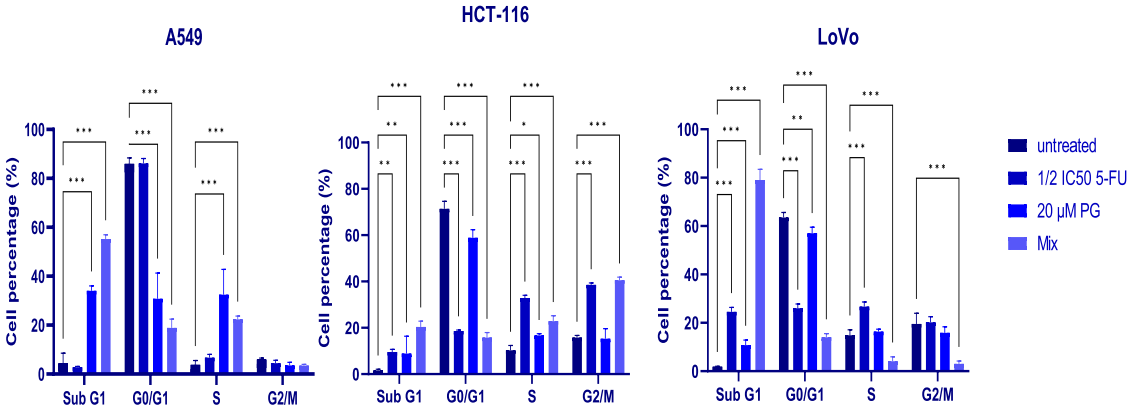

Figure 5. Representative of cell percentage profiles of cell-cycle distribution phases in cancer cell lines LoVo, HCT-116, and A549. Cells were exposed to 1/2 IC50 of 5-FU, 20 μM of PG, and Mix (1/2 IC50 of 5-FU + 20 μM of PG) for 48 h, and then DNA content was measured by flow cytometry. Experiments were performed in triplicate; results were presented as mean ± SD from three independent experiments (*p < 0.05; **p < 0.01; ***p < 0,001).

https://doi.org/10.1021/acsomega.4c04760
ACS Omega 2024, 9, 48112−48124

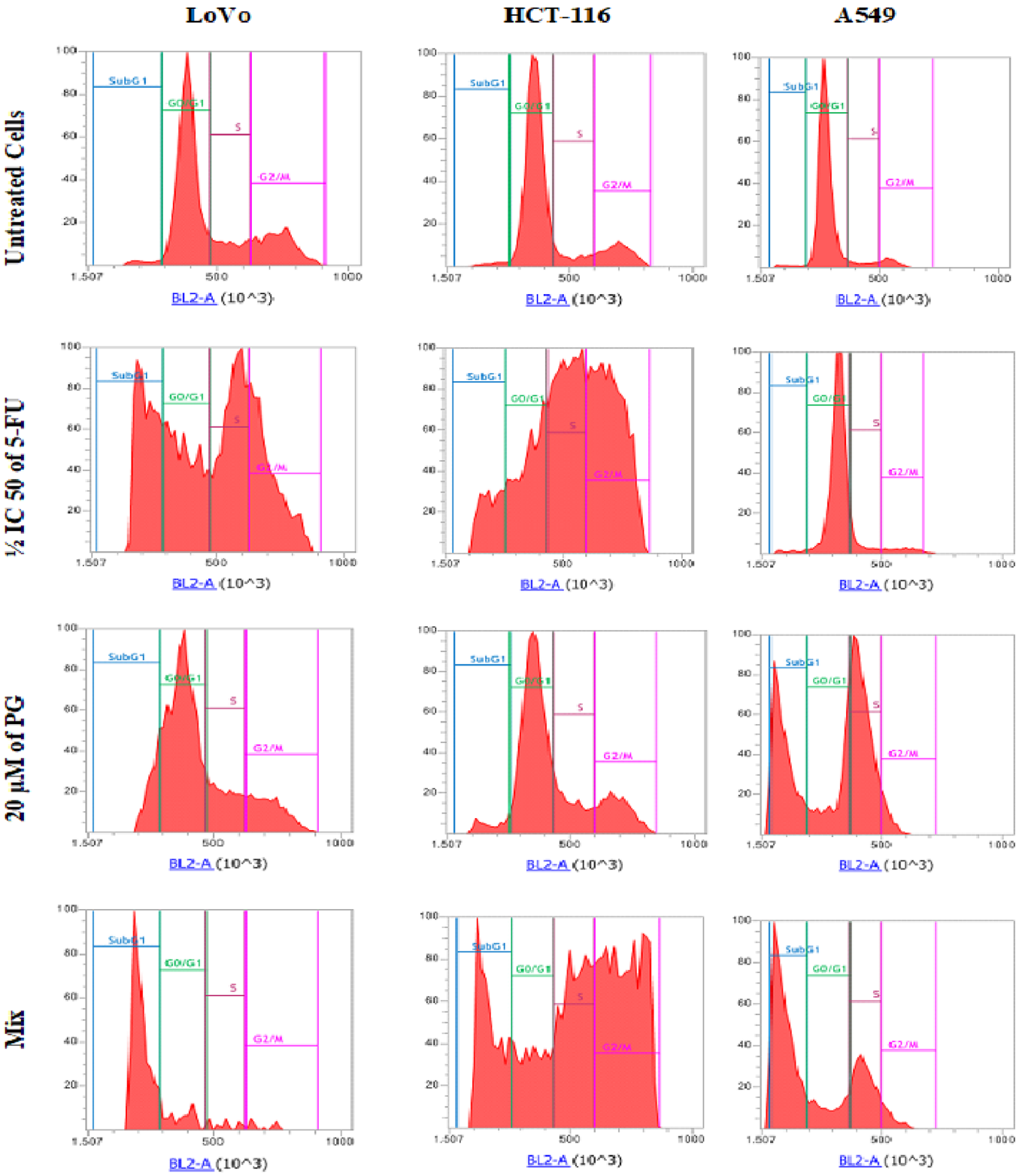

Figure 6. Representative profiles of cell-cycle distribution phases in cancer cell lines LoVo, HCT-116, and A549. Cells were exposed to 1/2 IC50 of 5-FU, 20 μM of PG, and Mix (1/2 IC50 of 5-FU + 20 μM of PG) for 48h, and then DNA content was measured by flow cytometry (*x*-axis: DNA content; *y*-axis: cell number). Experiments were performed in triplicate.

ligand molecules sourced from PubChem were subjected to optimization via molecular mechanics using the CHARMM27 force field, targeting a convergence criterion of a gradient of 0.01 kcal/(Å.mol). The resulting optimized structures were then saved in a mdb file format and compiled into a unified database. Both the receptor and ligand underwent 3D protonation in the Molecular Operating Environment (MOE) using its default protocols. This preparation phase included the addition of restraint tethers to specific atoms, annotation of ligand identifiers, incorporation of hydrogen atoms, and refinement

https://doi.org/10.1021/acsomega.4c04760
ACS Omega 2024, 9, 48112−48124

Table 2. Energy Interaction between Ligands and Akt

		ΔH		−TΔS		ΔG	
ligand	simulation N°	average	SD	average	SD	average	SD
IQO444	simulation 1	−43.61	8.04	19.27	0.05	−24.34	8.04
	simulation 2	−30.16	7.76	−1.67	0.05	−31.84	7.76
5957	simulation 1	−22.70	18.74	51.24	0.05	28.54	18.74
	simulation 2	−28.64	12.13	82.45	0.05	53.81	12.13
10196499	simulation 1	−26.42	7.48	36.93	0.05	10.51	7.48
	simulation 2	−16.95	5.82	16.86	3.34	−0.09	6.71
135455579	simulation 1	−18.17	4.78	12.36	4.80	−5.81	6.77
	simulation 2	−14.81	5.79	8.28	0.05	−6.53	5.79

of molecular coordinates. To identify potential binding sites, also referred to as cavities or active sites, the Site Finder function in MOE was employed. For the molecular docking procedure, the prepared ligand database was processed through MOE's DOCK module. The docking utilized the placement triangle matcher algorithm and employed London dG rescoring, generating a total of 100 poses. These poses were further refined using induced fit refinement and evaluated with GBVI/WSA dG scoring to select the top five binding poses for in-depth analysis with the objective of identifying the most favorable interaction for each ligand. Ultimately, the pose exhibiting the lowest energy was selected for subsequent investigations. Moreover, the docking poses and ligand interactions were viewed using MOE.[34]

Molecular Dynamic Simulations. The CHARMM-GUI platform was utilized for the preparation of input files by employing the CHARMM36 force field, which is well-suited for simulating biomolecular systems. (1) The initial structure of the Akt1-ligand complex was solubilized in a rectangular simulation box filled with water molecules, modeled using the TIP3P water model. (2) The system was then neutralized by adding appropriate amounts of potassium (K^+) and chloride (Cl^-) ions to maintain charge balance. (3) To alleviate any steric clashes and optimize the geometry of the system, energy minimization was performed using the steepest descent algorithm for 50,000 steps. (4) A pre-equilibration simulation was conducted for 125 ps in the NVT ensemble (constant number of particles, volume, and temperature) at 300 K (K). This step employed velocity rescaling with a stochastic term to stabilize the temperature. (5) Following pre-equilibration, the system underwent an NPT ensemble simulation for another 125 ps, maintaining constant particle number, pressure, and temperature. The pressure was regulated at 1 bar by using the C-rescale barostat. (6) The LINCS algorithm was implemented to maintain bond constraints throughout the simulation, ensuring stability of the molecular structure. (7) Periodic Boundary Conditions (PBC): To minimize edge effects and create an infinitely repeating system, periodic boundary conditions were applied in all three spatial dimensions (x, y, and z). (8) Interactions Modeling: Short-range van der Waals interactions were modeled using the Lennard−Jones (LJ) potential with a cutoff radius of 1.2 nm (nm). Long-range electrostatic interactions were computed using the particle-mesh Ewald (PME) algorithm with a real space cutoff of 1.2 nm. (9) Initial velocities of the particles were assigned based on Maxwell−Boltzmann distributions to initiate the dynamics of the system. (10) Two separate MD simulations were conducted, each lasting between 10 and 100 ns, with data sampling every 5 ns. This allowed for a detailed observation and analysis of the system's behavior over an extended period. (11) Postsimulation, various parameters were calculated to analyze the dynamics and interactions of the protein−ligand complex. These included roots-mean-square deviations (RMSD), residue root-mean-square fluctuations (RMSF), the number of hydrogen bonds, and the radius of gyration (Rg). This structured approach provides a robust framework for studying the behavior of protein−ligand complexes through molecular dynamics simulations, facilitating insights into their interactions and stability, which are crucial for drug design and development.[34]

Statistical Analysis. All of the assays were done in biological triplicate with three technical replicates, and data were given as mean ± standard deviation (SD). The statistical analysis was carried out through one-way and two-way analysis of variance (ANOVA) as well as Duncan's post hoc test using GraphPad Prism version 8 and Excel. A p-value of <0.05 was regarded as significant, and asterisks were used to indicate significance.

RESULTS

Evaluation of Combinatorial Chemotherapy Drug Toxicity in LoVo, HCT-116, and A549 Cells. The evaluation of chemotherapy drugs (oxaliplatin, paclitaxel, and 5-FU) showed different IC50 concentrations in LoVo, HCT-116, and A549 cells (Table 1). In LoVo cell line, the combinatorial treatment 1/2 IC50 5-FU + 1/2 IC50 paclitaxel showed an increase of cell viability (>80%), whereas the other two combinatorial treatments (1/2 IC50 of 5-FU + 1/2 IC50 of oxaliplatin and 1/2 IC50 of paclitaxel + 1/2 IC50 of oxaliplatin) showed no significative effect.

In the HCT-116 cell line, only the combinatorial treatment 1/2 IC50 oxaliplatin + 1/2 IC50 paclitaxel showed a significant effect. In contrast, in lung cancer cell line A549, the combinatorial treatment increased the toxicity effect of the three chemotherapy drugs (Figure 1).

Evaluation of the Toxicity of PG Alone and in Combination with Chemotherapy Drugs in LoVo, HCT-116, and A549 Cells. The evaluation of the PG potential on cell proliferation of cancer cells: LoVo, HCT-116, and A549 after 48h, using the MTT assay, showed an IC50 greater than 60 μM (Table 1). It is concluded that 5-FU and oxaliplatin had at least three times more toxic effect than PG against colon cancer cell lines (LoVo and HCT-116).

At a dose of 20 μM PG, over 80% of cell viability was obtained. The combinatorial treatment of 20 μM of PG + 1/2 IC50 of 5-FU after 48h showed a significant decrease in cell viability in all three cancer cell lines; LoVo:28%, HCT-116:32%, and A549:43% (Figure 2). However, the combination of 20 μM of PG + 1/2 IC50 of paclitaxel and oxaliplatin caused a percentage of cell viability greater than 50% after 48 h incubation (Figure 3). This study of the drug combination demonstrated that a clinically achievable concentration of PG (20 μM), which was

https://doi.org/10.1021/acsomega.4c04760
ACS Omega 2024, 9, 48112−48124

Table 3. Energy Decomposition Analysis (All Unit's kcal/mol): Poisson Boltzmann Model

ligand	simulation N°	VDWAALS		EEL		EPB		ENPOLAR		GGAS		GSOLV		TOTAL	
		average	SD	average	SD	average	SD	average	SD	average	SD	average	SD	average	SD
IQO444	simulation 1	−70.96	4.21	−181.72	19.38	215.59	16.42	−6.52	0.19	−252.68	21.42	209.07	16.46	−43.61	8.04
	simulation 2	−69.62	4.80	−190.65	18.79	236.95	18.06	−6.83	0.17	−260.28	22.53	230.12	18.16	−30.16	7.76
5957	simulation 1	−13.72	11.21	−199.54	221.60	193.63	200.16	−3.07	1.04	−213.26	216.41	190.56	200.60	−22.70	18.74
	simulation 2	−31.29	4.69	−234.58	98.31	241.88	88.78	−4.66	0.15	−265.87	97.90	237.23	88.77	−28.64	12.13
10196499		−62.95	8.26	−133.53	14.53	176.52	15.77	−6.45	0.26	−196.49	18.66	170.07	15.63	−26.42	7.48
	simulation 2	−61.90	2.97	−128.44	18.81	180.16	18.68	−6.78	0.16	−190.34	19.39	173.39	18.66	−16.95	5.82
135455579	simulation 1	−43.53	6.21	−14.71	5.19	44.90	7.16	−4.84	0.21	−58.23	5.96	40.06	7.07	−18.17	4.78
	simulation 2	−38.36	4.15	−9.28	6.83	37.70	7.93	−4.87	0.20	−47.64	5.68	32.82	7.92	−14.81	5.79

not cytotoxic to cells in culture, resulted in a significantly synergistic effect on 5-FU on both tested cell lines. A BrdU assay indicated that PG and 5-FU treatment inhibited the proliferation of HCT-116, LoVo, and A549 cells. The treatment using the mixture showed an improved inhibitory effect compared to the individual molecule (Figure 4).

Evaluation of Toxicity of PG and 5-FU in Hek293 Cells. To calculate the IC50 of the drugs for the cytotoxicity evaluation, nontumoral cells, Hek293, were exposed to different concentrations of PG and 5-FU (48h). At more than 100 μM, the PG treatment of HEK293 cells had no effects on cell proliferation while 5-FU exerted obvious antiproliferative effects on Hek293 cells in a dose-dependent manner (IC50 = 11.86 ± 2.23 μM).

PG and 5-FU Induced Cell-Cycle Arrest at SubG1. For the antiproliferation activity, the effect of PG on cell-cycle progression and apoptosis in LoVo, HCT-116, and A549 cells was investigated (Figures 5 and 6). After treatment with 20 μM PG for 48 h, the proportion of cells in the G0/G1 phase and S phase increased in the three cell lines, especially in A549 cells compared with the control. The treatment with 5-FU resulted in a significant reduction of the cell population in the S phase for human colon cancer cells (LoVo and HCT-116), while an increase in the S phase was observed in lung cancer cells (A549) compared to the results obtained with PG. The combination of 20 μM of PG and 1/2 IC50 of 5-FU caused a significant increase of cell percentage in the sub G1 phase.

Homology Modeling and Docking Analysis. The Akt1 model was subjected to molecular mechanics optimization using the CHARMM27 force field until a gradient of 0.01 kcal/(Å·mol) was achieved. Comparison of alpha-carbons between the template and optimized Akt1 models revealed a root-mean-square deviation (RMSD) of 1.726 Å. Evaluation of the Ramachandran plot statistics, conducted through PROCHECK software analysis, demonstrated that 97.7% of residues occupied the most favored or additional allowed regions in the model, indicating a favorable stereochemistry. The overall quality of the Akt1 model was further assessed using the ERRAT program, resulting in a quality factor of 81.92%, suggesting that the model is of reasonable quality.

Table 2 presents the results of docking studies between molecules PG (PubChem ID: 135455579), ATP (PubChem ID: 5957), Akt1 inhibitor VII (PubChem ID: 10196499) and IQO444, and the Akt1 in the tow simulations. Table 3 shows the different residue interactions of Akt1 and ligands and the binding energy. The 2D representation of the best docking poses of four ligands and their interactions at the active site of the Akt1-modeled structure is shown in Figure 7. The residues T81, L202, L210, L264, V270, Y272, R273, and F293, which were predominantly hydrophobic, were the most abundant regardless of the ligand.

Molecular Dynamic. *RMSD and Rg.* We assessed the thermodynamic equilibrium of our simulation systems using the root-mean-square deviation (RMSD) and the radius of gyration (Rg). These metrics were analyzed and are compared in Figures 8 and 9. RMSD values were tracked to evaluate the Akt1 protein stability during simulations. Fluctuations ranged from 0.4 to 0.8 nm for the IQO444/Akt1, ATP/Akt1, Akt1 inhibitor VII/Akt1, and PG/Akt1 complexes (Figure 9). Lower RMSD fluctuations implied greater structural stability and a likely attainment of thermodynamic equilibrium. Rg was computed to gauge the impact of ligands on the Akt1 compactness and receptor surface accessibility. Mean Rg values for Akt1 in the ligand complexes

https://doi.org/10.1021/acsomega.4c04760
ACS Omega 2024, 9, 48112−48124

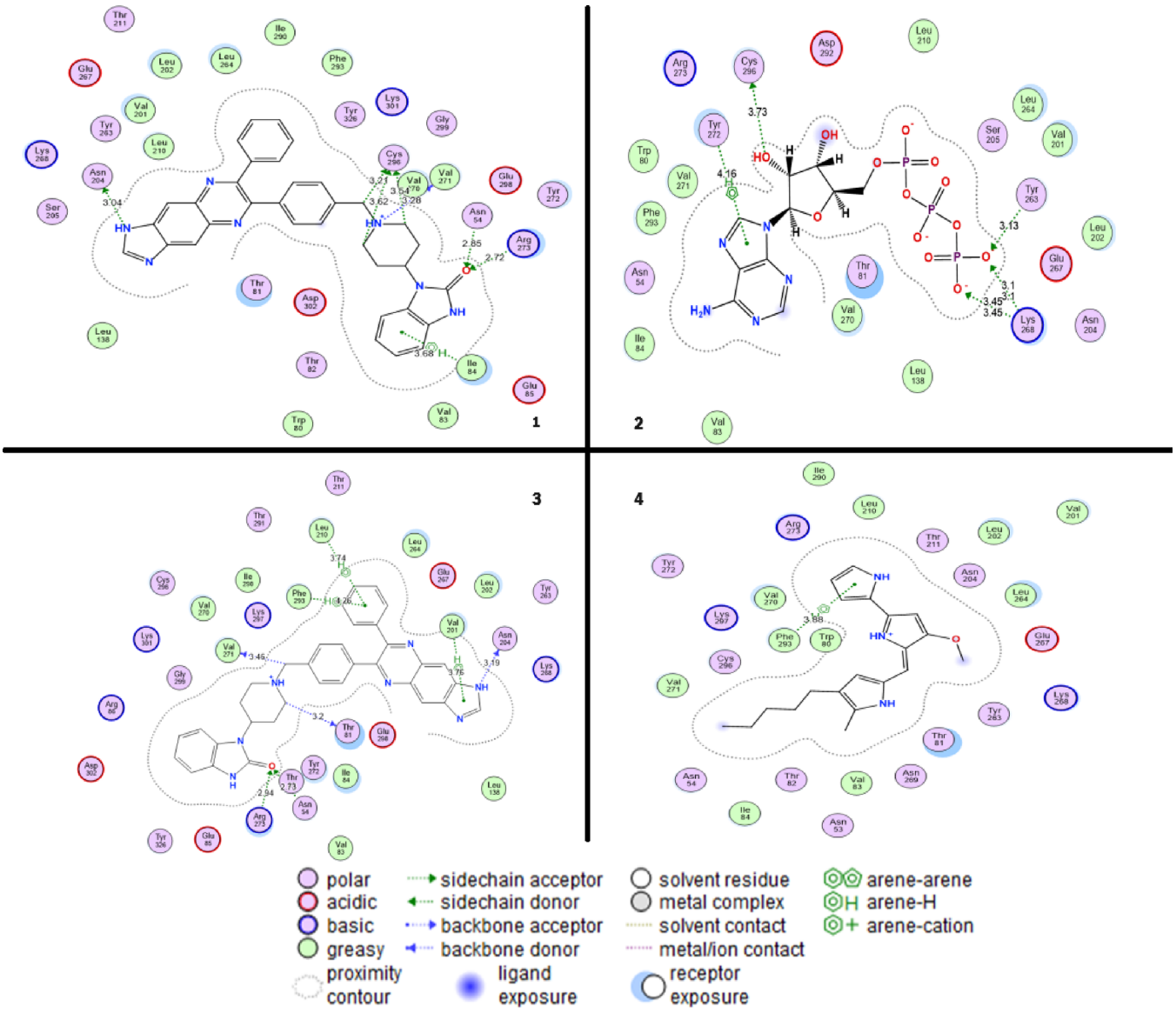

Figure 7. Molecular docking analysis; two-dimensional representation of interaction patterns of the Akt1-IQO444 complex (1); Akt1-ATP 5957 (2); Akt1-Akt1 inhibitor VII 10196499 (3); and Akt1-PG 135455579 (4).

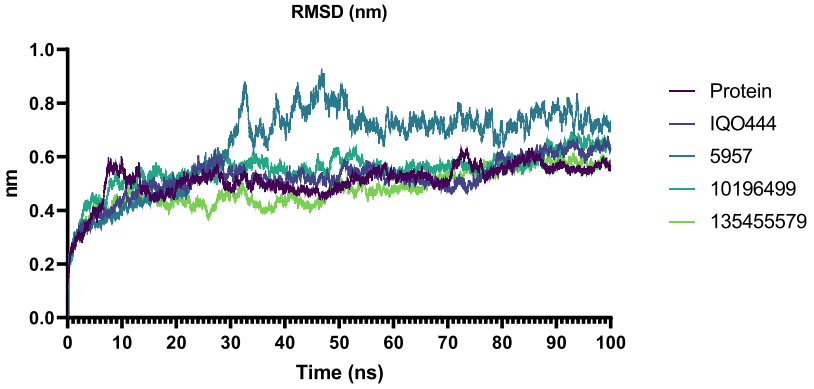

Figure 8. Molecular dynamics simulations trajectory analysis for RMSD in the backbone of the target protein bound with ligands root-mean-square deviations of Akt1 alone and Akt1 between the four ligands (experiments were performed in duplicate (simulations 1 and 2); results were presented as mean ± SD from two independent simulation).

ranged from 2.4 to 2.65 nm. Molecular dynamics studies provided insights into the enduring stability of ligands within the receptor's active site over the simulation period. Ligand binding to the protein is influenced by various factors, such as shape,

https://doi.org/10.1021/acsomega.4c04760
ACS Omega 2024, 9, 48112−48124

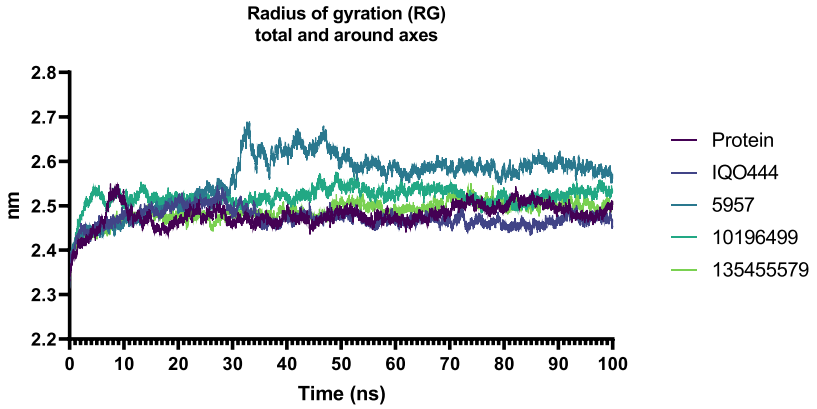

Figure 9. Molecular dynamics simulations trajectory analysis for the radius of the gyration graph (Rg) in the backbone of the target protein bound with ligands (experiments were performed in duplicate (simulations 1 and 2); results were presented as mean ± SD from two independent simulation).

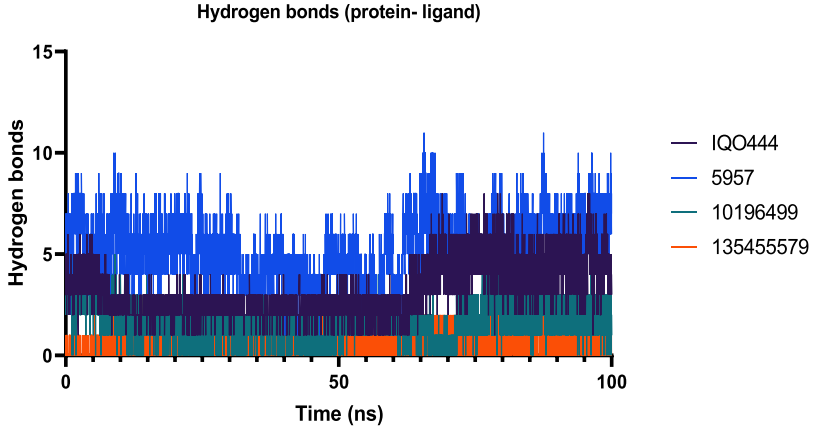

Figure 10. Molecular dynamics simulation trajectory analysis for hydrogen bonds formed between Akt1 and ligands (experiments were performed in duplicate (simulations 1 and 2); results were presented as mean ± SD from two independent simulation).

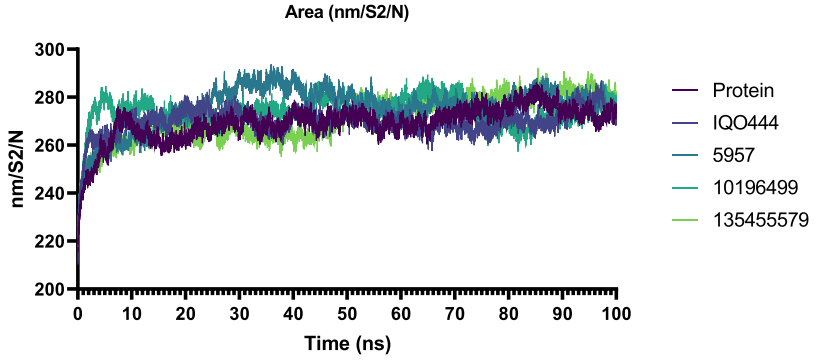

Figure 11. Molecular dynamics simulations trajectory analysis for the area (experiments were performed in duplicate (simulations 1 and 2); results were presented as mean ± SD from two independent simulation).

charge, and the molecular environment. Analysis of RMSD and Rg values suggested that while ligands decreased structural fluctuations of Akt1, compactness and accessible surface area remained largely unchanged. Taken together, these findings indicated that PG binding to Akt1 stabilized the structure without altering its overall shape and size (Figure 11).

Hydrogen Bonds and Binding. To investigate the interactions between ligands and proteins, we initially examined hydrogen bonds and subsequently evaluated the free energy of binding. These analyses utilized the Molecular Mechanics/Poisson−Boltzmann Surface Area (MM/PBSA) methods.

The distribution of hydrogen bonds between ligands and the Akt1 receptor varied, depending on the specific ligand−receptor pair. This variability in hydrogen bond formation also impacted the binding affinity of ligands for the receptor (Figure 10).

The MM/PBSA method, commonly employed for calculating binding free energies, decomposes the total free energy into molecular mechanics, solvation, and surface area components. Despite its computational expense, MM/PBSA provides more accurate estimates of binding free energies. ΔG_bind serves as a valuable tool for detailed atomistic analysis of ligand−protein interactions, which is particularly relevant for drug discovery applications.

https://doi.org/10.1021/acsomega.4c04760
ACS Omega 2024, 9, 48112−48124

Comparisons of average enthalpy (ΔH) values using the MM/PBSA method revealed statistically significant differences ($p < 0.05$) among the four ligands (IQO444, ATP, Akt1 inhibitor VII, and PG) concerning their interactions with Akt1.

RMSF. To elucidate structural changes induced by ligand binding, we computed the root-mean-square fluctuation (RMSF) of each residue with the results depicted in Figure 12. The active site comprises the following amino acids (N53

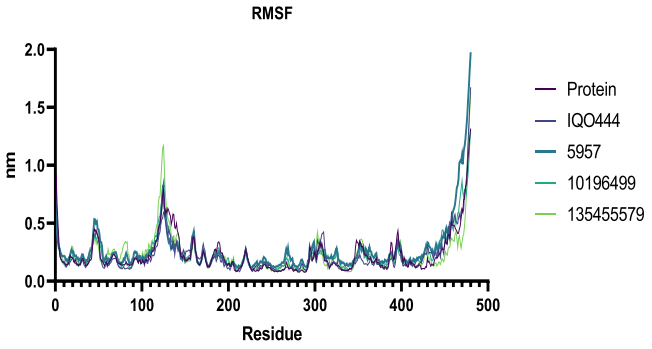

Figure 12. Molecular dynamics simulations trajectory analysis for RMSF in the backbone of the target protein bound with ligands (experiments were performed in duplicate (simulations 1 and 2); results were presented as mean ± SD from two independent simulation).

N54 W80 T81 T82 V83 I84 E85 R86 L138 V201 L202 N204 S205 L210 T211 Y263 L264 E267 K268 N269 V270 V271 Y272 R273 I290 T291 D292 F293 C296 K297 E298 G299 I300 K301 D302 Y326). RMSF analysis revealed comparable fluctuations among most residues across the four complex systems, indicating consistent binding of the compounds to the receptor. Remarkably, RMSF values for residues within the complexes were generally higher than those observed in the unbound protein, except for the region spanning residues 346−395 in the C-terminal region. Notably, a pronounced fluctuation of residues between Q113-P141 was observed in the complexed protein compared to the unbound protein, with this fluctuation being more pronounced in the presence of PG.

DISCUSSION

The proliferation and development of tumors involve multistep processes, and one of the most essential is the uncontrolled regulation of cell proliferation and cell apoptosis.[35] Currently, the reduction of proliferation and induction of cell apoptosis are the main therapeutic strategies in the treatment of cancer. Combinatorial treatment of chemotherapeutic agents is among the new cancer treatment strategies. Interestingly, this study confirmed a synergistic effect of oxaliplatin and paclitaxel in the treatment of colon cancer. The specific mechanism of synergy between oxaliplatin and paclitaxel is not fully understood, but it may involve enhanced disruption of cancer cell division and growth.[36,37] Studies investigating the synergistic effects of chemotherapy combinations are essential for optimizing treatment regimens and improving outcomes for cancer patients. Synergy between different drugs can enhance their effectiveness, potentially allowing for lower doses of each drug and reducing individual drug-related toxicities.

5-FU is a chemotherapeutic agent commonly used in the treatment of various types of cancer including colorectal, breast, and pancreatic cancers. However, its effectiveness can be limited by factors such as drug resistance and adverse side effects.[24,38,39] In our study, the combinatorial treatment of 5-FU and oxaliplatin or paclitaxel causes the increase in cellular toxicity. New studies are directed toward the combination of chemotherapeutic drugs.

There has been some research interest in studying the potential anticancer properties of natural compounds including PG. Previous studies have suggested that PG was capable to induce apoptosis as well as to suppress proliferation in HCT-116 and LoVo cells.[24] In this study, the effect of PG as an anticancer molecule against HTCT-116, LoVo, and A549 cancer cells was confirmed. Besides, PG significantly inhibited, in a dose-dependent manner, the proliferation and induced apoptosis in human colon and lung cancer cells. Notably, almost complete inhibition can be achieved at high concentrations.

It becomes more interesting to involve natural products in the combinatory treatment of cancer cells. The present study showed that the combination of PG with 5-FU, oxaliplatin, and paclitaxel increased the toxicity effect of chemotherapy agents in cancer cell lines. Moreover, PG significantly suppressed cell proliferation and induced cell apoptosis, in combination with a low dose of 5-FU (1/2 IC50). PG significantly strengthened 5-FU therapeutic efficacy in human cell cancer types, corroborating findings from previous studies.[37]

The synergistic effect of combining 5-FU with isolated natural compounds in cancer inhibition is an area of growing interest in cancer research and treatment. Researchers have explored the combination of 5-FU with various natural compounds derived from plants, herbs, and other sources to enhance its therapeutic potential and improve cancer treatment outcomes. In fact, some common natural compounds exhibited synergistic effects with 5-FU. For instance, curcumin was reported to sensitize colorectal cancer cells to 5-FU, making them more susceptible to the drug's effects.[40] Resveratrol, found in grapes, berries, and peanuts, has been shown to induce apoptosis in cancer colorectal cells and enhance the efficacy of 5-FU.[41] Likewise, epigallocatechin gallate, a potent antioxidant found in green tea, has been reported to enhance the antitumor effects of 5-FU and reduce drug resistance in cancer cells.[42] Besides, quercetin, present in fruits and vegetables, was able to enhance the cytotoxic effects of 5-FU in colorectal cancer cells[43] while genistein, found in soybeans, has been evaluated for its ability to potentiate the sensitivity of cancer cells to 5-FU treatment.[44]

It has been reported that the antiproliferation of PG was associated with cell-cycle arrest in phase S. The present investigation demonstrated that PG induced cell-cycle arrest not only at the S phase but also at the G0/G1 phase in HCT-116, LoVo, and A549 cells. The mechanisms by which PG exerts above bioactivity are still unclear, while 5-FU exerts an anticancer activity through thymidylate synthase inhibition and incorporation into RNA and DNA.[45]

The current docking investigation clearly indicated that PG was capable of inhibiting Akt1, potentially explaining the proapoptotic effect observed by altering the flexibility of the Q113-P141 region. Our findings supported a direct interaction of PG with Akt1 and favored an apoptosis induction due to an inhibition of PI3 kinase/Phospho-Akt signaling.[46] Indeed, in silico docking studies have identified the ATP binding site of Akt as a significant interaction point for PG suggesting that PG effectively bound to this site, thereby preventing Akt activation. The docking data also indicated that PG could significantly interfere with the activity of multiple kinases, including Akt, which is critical for its anticancer effects,[47,48] The inhibition of Akt1 by PG is part of a broader mechanism where it also targets

https://doi.org/10.1021/acsomega.4c04760
ACS Omega 2024, 9, 48112−48124

the mTOR pathway, further contributing to its anticancer properties.[46−48]

In general, the underlying mechanisms for the synergetic effects of natural compounds with 5-FU are still being studied, but they are believed to involve multiple pathways, such as enhancing apoptosis, inhibiting cell proliferation, and modulating drug resistance mechanisms.[25,49]

Interestingly, the combinatory treatment could help reduce the dosage and toxicity of the chemotherapy drug, which can be beneficial for patients, especially those who cannot tolerate high doses of 5-FU alone. However, it is worthy to note that the use of natural compounds in combination with chemotherapy should be approached with caution and under the supervision of medical professionals. The combination (PG + 5-FU) allowed synergistic effects of both drugs, as well as a reduction of 5-FU doses in cancer and normal cells, which is another advantage in addition to the improved efficacy. This synergistic effect allowed minimizing side effects compared to higher doses of 5-FU alone or in combination with other agents. The combination of PG + 5-FU likely exhibited the best synergistic effect due to their complementary mechanisms of action; PG's ability to enhance the cytotoxic effects of 5-FU, and the potential to overcome resistance mechanisms. It seemed that targeting Akt1 by PG might potentiate the action of 5-FU. Therefore, this multifaceted attack on cancer cells could explain why this combination outperforms others in the current study.

CONCLUSIONS

The combination of chemotherapy drugs with natural compounds like PG, an anticancer tripyrrole red pigment produced by microorganisms such as *Serratia marcescens*, showed promising results in enhancing the cytotoxic effects against tumor cells, particularly in colon and lung cancers. PG, while having a limited effect on cell viability when used alone, significantly boosted the efficacy of chemotherapeutic agents primarily used in colon and lung cancer treatment, such as 5-FU. The current study indicated that addition of 20 μM PG to 5-FU resulted in a notable increase in cell viability inhibition of various cancer cell lines. Interestingly, a low dose of 5-FU (1/2 IC50 of 5-FU) alone inhibited cell viabilities by 36, 35, and 30% in LoVo, HCT-116, and A549 cells, respectively. However, the inclusion of PG raised the inhibition levels to over 65% in these cells, demonstrating a synergistic effect between PG and 5-FU. In contrast, PG alone inhibited less than 14% of cell viability, highlighting its role as a potentiator rather than a primary treatment agent. In the future, other natural products from medicinal plants and microbial bioactive molecules should be evaluated in combination with known chemotherapeutic compounds to select better synergistic anticancer effects. Additionally, further investigations into the molecular mechanisms of PG, particularly its interactions with signaling pathways, are necessary.

AUTHOR INFORMATION

Corresponding Author

Abir Ben Bacha − *Biochemistry Department, Science College, King Saud University, Riyadh 11495, Saudi Arabia;* orcid.org/0000-0001-6372-7483; Email: aalghanouchi@ksu.edu.sa

Authors

Fares Elghali − *Laboratory of Molecular and Cellular Screening Processes, Centre of Biotechnology of Sfax, Sfax 3038, Tunisia*

Dhouha Msalbi − *Laboratory of Molecular and Cellular Screening Processes, Centre of Biotechnology of Sfax, Sfax 3038, Tunisia*

Fakher Frikha − *Laboratory of Molecular and Cellular Screening Processes, Centre of Biotechnology of Sfax, Sfax 3038, Tunisia*

Mona Alonazi − *Biochemistry Department, Science College, King Saud University, Riyadh 11495, Saudi Arabia;* orcid.org/0000-0002-9430-7980

Emna Sahli − *Unity of Analysis, Centre of Biotechnology of Sfax, Sfax 3038, Tunisia*

Bochra Hakim − *Laboratory of Molecular and Cellular Screening Processes, Centre of Biotechnology of Sfax, Sfax 3038, Tunisia*

Sami Mnif − *Laboratory of Molecular and Cellular Screening Processes, Centre of Biotechnology of Sfax, Sfax 3038, Tunisia*

Sami Aifa − *Laboratory of Molecular and Cellular Screening Processes, Centre of Biotechnology of Sfax, Sfax 3038, Tunisia*

Complete contact information is available at: https://pubs.acs.org/10.1021/acsomega.4c04760

Notes

The authors declare no competing financial interest.

ACKNOWLEDGMENTS

The authors extend their appreciation to the research's Supporting Project number (RSP2024R237), King Saud University, Riyadh, Saudi Arabia, for partially funding this work.

REFERENCES

(1) Metro, G.; Finocchiaro, G.; Toschi, L.; Bartolini, S.; Magrini, E.; Cancellieri, A.; et al. Epidermal growth factor receptor (EGFR) targeted therapies in non-small cell lung cancer (NSCLC). *Rev. Recent Clin Trials* **2006**, *1*, 1−13.

(2) Zhang, T.; Wan, B.; Zhao, Y.; Li, C.; Liu, H.; Lv, T.; et al. Treatment of uncommon EGFR mutations in non-small cell lung cancer: new evidence and treatment. *Cancer Res.* **2019**, *8*, 302.

(3) Mittal, V; El Rayes, T; Narula, N; McGraw, T. E.; Altorki, N. K.; Barcellos-Hoff, M. H. The Microenvironment of Lung Cancer and Therapeutic Implications. In *Lung Cancer and Personalized Medicine: Novel Therapies and Clinical Management*; Ahmad, A; Gadgeel, S. M., editors, Springer International Publishing: Cham, 2016, p 75−110. .

(4) Tan, Z.; Xue, H.; Sun, Y.; Zhang, C.; Song, Y.; Qi, Y. The Role of Tumor Inflammatory Microenvironment in Lung Cancer. *Front. Pharmacol.* **2021**, *12*, No. 688625.

(5) Gout, S.; Huot, J. Role of Cancer Microenvironment in Metastasis: Focus on Colon Cancer. *Cancer Microenvironment* **2008**, *1*, 69−83.

(6) Jahanafrooz, Z.; Mosafer, J.; Akbari, M.; Hashemzaei, M.; Mokhtarzadeh, A.; Baradaran, B. Colon cancer therapy by focusing on colon cancer stem cells and their tumor microenvironment. *Journal of Cellular Physiology* **2020**, *235*, 4153−66.

(7) Liu, J.; Lan, Y.; Tian, G.; Yang, J. A Systematic Framework for Identifying Prognostic Genes in the Tumor Microenvironment of Colon Cancer. *Front. Oncol.* **2022**, *12*, No. 899156.

(8) Reuvers, T. G. A.; Kanaar, R.; Nonnekens, J. DNA Damage-Inducing Anticancer Therapies: From Global to Precision Damage. *Cancers (Basel)* **2020**, *12*, 2098.

(9) Baguley, B. C.; Drummond, C. J.; Chen, Y. Y.; Finlay, G. J. DNA-Binding Anticancer Drugs: One Target. *Two Actions. Molecules* **2021**, *26*, 552.

(10) Balayssac, D.; Durif, J.; Lambert, C.; Dalbos, C.; Chapuy, E.; Etienne, M.; et al. Exploring Serum Biomarkers for Neuropathic Pain in Rat Models of Chemotherapy-Induced Peripheral Neuropathy: A Comparative Pilot Study with Oxaliplatin, Paclitaxel, Bortezomib, and Vincristine. *Toxics* **2023**, *11*, 1004.

(11) Attal, N.; Bouhassira, D.; Gautron, M.; Vaillant, J. N.; Mitry, E.; Lepère, C.; et al. Thermal hyperalgesia as a marker of oxaliplatin neurotoxicity: A prospective quantified sensory assessment study. *Pain* **2009**, *3*, 245−252.
(12) Li, M.-H.; Ito, D.; Sanada, M.; Odani, T.; Hatori, M.; Iwase, M.; et al. Effect of 5-fluorouracil on G1 phase cell cycle regulation in oral cancer cell lines. *Oral Oncology* **2004**, *40*, 63−70.
(13) Maybaum, J.; Ullman, B.; Mandel, H. G.; Day, J. L.; Sadee, W. Regulation of RNA- and DNA-directed Actions of 5-Fluoropyrimidines in Mouse T-Lymphoma (S-49) Cells. *Cancer Res.* **1980**, *40*, 4209−4215.
(14) Sethy, C.; Kundu, C. N. 5-Fluorouracil (5-FU) resistance and the new strategy to enhance the sensitivity against cancer: Implication of DNA repair inhibition. *Biomedicine & Pharmacotherapy* **2021**, *137*, No. 111285.
(15) Lazic, J.; Skaro Bogojevic, S.; Vojnovic, S.; Aleksic, I.; Milivojevic, D.; Kretzschmar, M.; et al. Synthesis, Anticancer Potential and Comprehensive Toxicity Studies of Novel Brominated Derivatives of Bacterial Biopigment Prodigiosin from Serratia marcescens ATCC 27117. *Molecules* **2022**, *27*, 3729.
(16) Darshan, N.; Manonmani, H. K. Prodigiosin and its potential applications. *J. Food Sci. Technol.* **2015**, *52*, 5393−407.
(17) Jardak, M.; Atoissi, A.; Msalbi, D.; Atoui, D.; Bouizgarne, B.; Rigane, G.; et al. Antibacterial, antibiofilm and cytotoxic properties of prodigiosin produced by a newly isolated Serratia sp. C6LB from a milk collection center. *Microbial Pathogenesis* **2022**, *164*, No. 105449.
(18) Mnif, S.; Jardak, M.; Bouizgarne, B.; Aifa, S. Prodigiosin from Serratia: Synthesis and potential applications. *Asian Pac. J. Trop. Biomed.* **2022**, *12*, 233−242.
(19) Chiu, W.-J.; Lin, S.-R.; Chen, Y.-H.; Tsai, M.-J.; Leong, M. K.; Weng, C.-F. Prodigiosin-Emerged PI3K/Beclin-1-Independent Pathway Elicits Autophagic Cell Death in Doxorubicin-Sensitive and -Resistant Lung Cancer. *J. Clin Med.* **2018**, *7*, 321.
(20) Manderville, R. A. Synthesis, proton-affinity and anti-cancer properties of the prodigiosin-group natural products. *Curr. Med. Chem. Anticancer Agents* **2001**, *1*, 195−218.
(21) Elahian, F.; Moghimi, B.; Dinmohammadi, F.; Ghamghami, M.; Hamidi, M.; Mirzaei, S. A. The Anticancer Agent Prodigiosin Is Not a Multidrug Resistance Protein Substrate. *DNA and Cell Biology* **2013**, *32*, 90−7.
(22) Zhao, W.; Gao, D.; Ning, L.; Jiang, Y.; Li, Z.; Huang, B.; et al. Prodigiosin inhibits the proliferation of glioblastoma by regulating the KIAA1524/PP2A signaling pathway. *Sci. Rep* **2022**, *12*, 18527.
(23) Wang, X.; Cui, Z.; Zhang, Z.; Zhao, J.; Liu, X.; Meng, G.; et al. Two-Step Optimization for Improving Prodigiosin Production Using a Fermentation Medium for Serratia marcescens and an Extraction Process. *Fermentation* **2024**, *10*, 85.
(24) Zhao, C.; Qiu, S.; He, J.; Peng, Y.; Xu, H.; Feng, Z.; et al. Prodigiosin impairs autophagosome-lysosome fusion that sensitizes colorectal cancer cells to 5-fluorouracil-induced cell death. *Cancer Letters* **2020**, *481*, 15−23.
(25) Lei, Z. N.; Tian, Q.; Teng, Q. X.; Wurpel, J. N. D.; Zeng, L.; Pan, Y.; et al. Understanding and targeting resistance mechanisms in cancer. *MedComm* **2020**, *4* (3), No. e265.
(26) Fernández, J.; Silván, B.; Entrialgo-Cadierno, R.; Villar, C. J.; Capasso, R.; Uranga, J. A.; et al. Antiproliferative and palliative activity of flavonoids in colorectal cancer. *Biomedicine & Pharmacotherapy* **2021**, *143*, No. 112241.
(27) Gelen, V.; Şengül, E.; Yıldırım, S.; Senturk, E.; Tekin, S.; Kükürt, A. The protective effects of hesperidin and curcumin on 5-fluorouracil−induced nephrotoxicity in mice. *Environ. Sci. Pollut Res.* **2021**, *28*, 47046−55.
(28) Wan, Y.; Wang, J.; Xu, J.; Tang, F.; Chen, L.; Tan, Y.; et al. Panax ginseng and its ginsenosides: potential candidates for the prevention and treatment of chemotherapy-induced side effects. *J. Ginseng Res.* **2021**, *45*, 617−30.
(29) Choura, E.; Elghali, F.; Bernard, P. J.; Msalbi, D.; Marco-Contelles, J.; Aifa, S.; et al. Benzochromenopyrimidines: Synthesis, Antiproliferative Activity against Colorectal Cancer and Physicochemical Properties. *Molecules* **2022**, *27*, 7878.
(30) Zhou, M.; Xi, J.; Cheng, Y.; Sun, D.; Shu, P.; Chi, S.; et al. Reprogrammed mesenchymal stem cells derived from iPSCs promote bone repair in steroid-associated osteonecrosis of the femoral head. *Stem Cell Res. Ther* **2021**, *12*, 175.
(31) Liu, J.; Peng, Y.; Wei, W. Cell cycle on the crossroad of tumorigenesis and cancer therapy. *Trends Cell Biol.* **2022**, *32*, 30−44.
(32) Laskowski, R. A.; MacArthur, M. W.; Moss, D. S.; Thornton, J. M. PROCHECK: a program to check the stereochemical quality of protein structures. *J. Appl. Crystallogr.* **1993**, *26*, 283−91.
(33) Colovos, C.; Yeates, T. O. Verification of protein structures: Patterns of nonbonded atomic interactions. *Protein Sci.* **1993**, *2*, 1511−9.
(34) Frikha, F.; Jardak, M.; Aifa, S.; Mnif, S. A novel perspective on eugenol as a natural anti-quorum sensing molecule against Serratia sp. *Microb Pathog* **2024**, *189*, No. 106576.
(35) Brown, J. M.; Attardi, L. D. The role of apoptosis in cancer development and treatment response. *Nat. Rev. Cancer* **2005**, *5*, 231−7.
(36) Taieb, J.; Seufferlein, T.; Reni, M.; Palmer, D. H.; Bridgewater, J. A.; Cubillo, A.; et al. Treatment sequences and prognostic/predictive factors in metastatic pancreatic ductal adenocarcinoma: univariate and multivariate analyses of a real-world study in Europe. *BMC Cancer* **2023**, *23*, 877.
(37) Dominiak, H. S. H.; Hasselsteen, S. D.; Nielsen, S. W.; Andersen, J. R.; Herrstedt, J. Prevention of Taste Alterations in Patients with Cancer Receiving Paclitaxel- or Oxaliplatin-Based Chemotherapy-A Pilot Trial of Cannabidiol. *Nutrients* **2023**, *15*, 3014.
(38) Hsieh, H.-Y.; Shieh, J.-J.; Chen, C.-J.; Pan, M.-Y.; Yang, S.-Y.; Lin, S.-C.; et al. Prodigiosin down-regulates SKP2 to induce p27KIP1 stabilization and antiproliferation in human lung adenocarcinoma cells. *Br. J. Pharmacol.* **2012**, *166*, 2095−108.
(39) Liu, Y.; Zhou, H.; Ma, X.; Lin, C.; Lu, L.; Liu, D.; et al. Prodigiosin Inhibits Proliferation, Migration, and Invasion of Nasopharyngeal Cancer Cells. *Cellular Physiology and Biochemistry* **2018**, *48*, 1556−62.
(40) Li, G.; Fang, S.; Shao, X.; Li, Y.; Tong, Q.; Kong, B.; et al. Curcumin Reverses NNMT-Induced 5-Fluorouracil Resistance via Increasing ROS and Cell Cycle Arrest in Colorectal Cancer Cells. *Biomolecules* **2021**, *11*, 1295.
(41) Chung, S. S.; Dutta, P.; Austin, D.; Wang, P.; Awad, A.; Vadgama, J. V. Combination of resveratrol and 5-flurouracil enhanced anti-telomerase activity and apoptosis by inhibiting STAT3 and Akt signaling pathways in human colorectal cancer cells. *Oncotarget* **2018**, *9*, 32943−57.
(42) La, X.; Zhang, L.; Li, Z.; Li, H.; Yang, Y. (−)-Epigallocatechin Gallate (EGCG) Enhances the Sensitivity of Colorectal Cancer Cells to 5-FU by Inhibiting GRP78/NF-κB/miR-155−5p/MDR1 Pathway. *J. Agric. Food Chem.* **2019**, *67*, 2510−8.
(43) Dai, W.; Gao, Q.; Qiu, J.; Yuan, J.; Wu, G.; Shen, G. Quercetin induces apoptosis and enhances 5-FU therapeutic efficacy in hepatocellular carcinoma. *Tumor Biol.* **2016**, *37*, 6307−13.
(44) Suzuki, R.; Kang, Y.; Li, X.; Roife, D.; Zhang, R.; Fleming, J. B. Genistein potentiates the antitumor effect of 5-fluorouracil by inducing apoptosis and autophagy in human pancreatic cancer cells. *Anticancer Res.* **2014**, *34*, 4685−4692.
(45) Longley, D. B.; Harkin, D. P.; Johnston, P. G. 5-Fluorouracil: mechanisms of action and clinical strategies. *Nat. Rev. Cancer* **2003**, *3*, 330−8.
(46) Paul, T.; Bhardwaj, P.; Mondal, A.; Bandyopadhyay, T. K.; Mahata, N.; Bhunia, B. Identification of Novel Protein Targets of Prodigiosin for Breast Cancer Using Inverse Virtual Screening Methods. *Appl. Biochem. Biotechnol.* **2023**, *195*, 7236−7254.
(47) Espona-Fiedler, M.; Soto-Cerrato, V.; Hosseini, A.; Lizcano, J. M.; Guallar, V.; Quesada, R.; et al. Identification of dual mTORC1 and mTORC2 inhibitors in melanoma cells: Prodigiosin vs. obatoclax. *Biochem. Pharmacol.* **2012**, *83*, 489−96.
(48) Mohamed, W. A.; El-Nekhily, N. A.; Mahmoud, H. E.; Hussein, A. A.; Sabra, S. A. Prodigiosin/celecoxib-loaded into zein/sodium

https://doi.org/10.1021/acsomega.4c04760
ACS Omega 2024, 9, 48112−48124

caseinate nanoparticles as a potential therapy for triple negative breast cancer. *Sci. Rep* **2024**, *14*, 181.
(49) Wang, X.; Zhang, H.; Chen, X. Drug resistance and combating drug resistance in cancer. *Cdr* **2019**, *2*, 141−60.

https://doi.org/10.1021/acsomega.4c04760
ACS Omega 2024, 9, 48112−48124